Applied Thermal Engineering 178 (2020) 115617

Contents lists available at ScienceDirect

Applied Thermal Engineering

journal homepage: www.elsevier.com/locate/apthermeng

Thermodynamic optimization of Rankine cycle using CO_2-based binary zeotropic mixture for ocean thermal energy conversion

Chengyu Li[a], Lisheng Pan[b,*], Yongzhen Wang[c,**]

[a] School of Transportation and Vehicle Engineering, Shandong University of Technology, Zibo 255000, China
[b] State Key Laboratory of High-temperature Gas Dynamics, Institute of Mechanics, Chinese Academy of Sciences, Beijing 100190, China
[c] Department of Electrical Engineering, Energy Internet Research Institute, Tsinghua University, Beijing 100084, China

HIGHLIGHTS

- CO_2-based binary zeotropic mixtures are studied for converting ocean thermal energy.
- These fluids have potential to improve coupling of thermodynamic cycle and seawater.
- Comparison, evaluation and optimization are carried out on several mixture fluids.

ARTICLE INFO

Keywords:
OTEC (Ocean Thermal Energy Conversion)
CO_2-based mixture
Performance evaluation
Optimization design

ABSTRACT

This work provides an exploration on improving the performance of a closed ocean thermal energy conversion (OTEC) system. In order to approach the Lorenz cycle and obtain better thermal matching, a Rankine cycle using CO_2-based binary zeotropic mixtures is considered. Six organic working fluids, including R134a, R152a, R161, R1234yf, R1234ze(E) and R32, are selected to be additives for binary mixtures, in addition, various concentrations of CO_2 are investigated in order to obtain varying temperature glide. Besides, pure working fluids, including NH_3 and CO_2, are also comparatively investigated with the mixtures. The specific net power output and thermal efficiency are used to evaluate OTEC thermodynamic performance, and the ratio of net power output to total heat transfer area is adopted for a preliminary economic analysis. Different effects on cycle performance are analyzed. Finally, an overall optimization to maximize the system thermal efficiency and specific work are carried out, respectively. The simulation is based on a designed Matlab program. The results indicate that CO_2-based binary zeotropic mixtures could improve thermodynamic coupling of cycle and external seawater, achieving a deeper heat utilization of warm/cold seawater than that of pure working fluid. The performance of Rankine cycle is affected by the mixture composition, and composition at which mixture has evaporating temperature glide of 7–8 °C is recommended. The binary mixtures produce larger specific power output than pure working fluids, and CO_2/R32 (0.76/0.24 wt%) produces the maximum value of 0.696 kJ/kg, nearly 38% higher than that of pure NH_3. Although the mixtures are inferior to NH_3 according to preliminary economic analysis. The thermodynamic findings still prove that Rankine cycle with CO_2-based binary mixture is a promising alternative for OTEC system.

1. Introduction

The ocean is the largest energy store on Earth, and offers inexhaustible sources of renewable energy. The thermal gradient between warm surface water and cold deep ocean water is sufficient for the OTEC (ocean thermal energy conversion) system to drive a heat engine power cycle and generate power. It is estimated that the maximum OTEC net power production is about 30 TW, with net power density ranging from about 500 to 1000 kW/km^2 [1]. The first demonstrative 50 kW Mini-OTEC offshore plant was constructed in Hawaii in 1979, using ammonia as working fluid [2]. Saga University constructed an onshore demonstration 100 kW OTEC plant on the Coast of Nauru Island in 1981, with R22 as working fluid. Recently, a 100 kW OTEC plant using R134a was operated in Kumejima island of Japan in 2013, and a 100 kW plant was connected to the electric grid in Hawaii in 2015 [3]. Many other projects are currently under development throughout

* Corresponding author.
** Corresponding author.
E-mail addresses: panlisheng@imech.ac.cn (L. Pan), wyz80hou@mail.tsinghua.edu.cn (Y. Wang).

https://doi.org/10.1016/j.applthermaleng.2020.115617
Received 8 December 2019; Received in revised form 13 June 2020; Accepted 16 June 2020
Available online 23 June 2020

Nomenclature

c_p	specific heat, kJ/(kg·K)
g	gravitational acceleration, m/s^2
h	specific enthalpy, kJ/kg
K	absolute roughness, um
$\dot{m}$	mass flow rate, kg/s
p	pressure, MPa
$\dot{Q}$	heat flow rate, kW
T	temperature, °C
U	overall heat transfer coefficient
$\dot{W}$	power produced or consumed, kW
x	mass fraction

Subscripts

cond	condensing
cs	cold seawater
evap	evaporating
g	gas
l	liquid
in	inlet
max	maximum
min	minimum
out	outlet
p	pump
pp	pinch point
s	isentropic
sys	system
t	turbine
ws	warm seawater

Greek symbols

ρ	density, kg/m^3
γ	gamma parameter, kW/m^2
η	efficiency

the world. For example, a 10–25 MW offshore OTEC power plant in Curaçao is planned by Ecopark, the design of plant and effects of seawater fluctuations have been finished [4]. DCNS is planning to build a 16 MW OTEC plant in Martinique Island, it is expected to be operated in the summer of 2020 [5]. Although technical feasibility has been demonstrated by several pilot plants, the OTEC tech faces many challenges, and has not been economically applied until now, even so, interest in this renewable technology has been sustained.

In view of the low temperature difference between surface and deep sea water, which is only 20–25 °C even in tropical area, thermal efficiency of OTEC is in the order of 3–5% at best [6]. The OTEC system shows more temperature sensitivity, which a variation of 1 °C in the seawater thermal resource corresponds to a change in net power output of the order of 15% [1]. Therefore, under the limited external conditions, study to improve thermodynamic performance of OTEC system is one way of the utmost importance. Many researchers have contributed their efforts in cycle design and fluids selection. Uehara [7] performed optimization study for a closed OTEC system using ammonia as working fluid. To improve cycle thermal efficiency, Uehara further presented a new closed cycle system named Uehara Cycle [8]. Yoon et al. [9] proposed an ejector pump OTEC (EP-OTEC) configuration using R152a as working fluid which yields 38% higher system efficiency than a basic OTEC cycle. To improve cycle thermodynamic performance, Ikegami et al. [10] investigated a double-stage Rankine cycle, using R134a and ammonia as working fluid. Influence of reduction of the irreversible losses in the heat exchange process on the system performance was investigated, and results indicate that the double-stage Rankine cycle can improve the power output by reducing the irreversible losses in heat exchange process. Sun et al. [11] performed theoretical optimization of OTEC to maximize the net power output, using NH_3 and R134a as working fluid. Yang et al. [12] conducted a thermodynamic performance optimization using five working fluids. The ratio of net power output to total heat transfer area was introduced to evaluate the objective parameter. Results indicate that NH_3 performs optimally in objective parameter evaluation, while R600a yields the highest thermal efficiency. A multi-objective optimization of OTEC system using six working fluids was carried out by Wang et al. [13], considering levelized cost of energy and exergy efficiency as two objective functions. The results show that NH_3 and R601 have the best performance. Yoon et al. [14] conducted screening of working fluids in a subcritical OTEC power cycle based on thermal efficiency and main component size requirement. Results indicate that NH_3 is the preferred working fluid. However, these commonly investigated working fluids for OTEC may suffer from environmental or safety defects, for example, NH_3 is toxic, flammable and incompatible with copper.

In order to improve thermodynamic performance of OTEC system, additional heat sources, such as waste heat from nuclear power plant condenser effluent [15], geothermal waste heat [16], and solar energy [6,17], were incorporated to increase the temperature of warm seawater. In addition, some researchers also performed experimental researches on OTEC system. A newly designed closed cycle demonstration OTEC plant using R134a was built by Faizal et al. [18] to experimentally investigate the system performance at different operating conditions, and a maximum efficiency of about 1.5% was achieved in the system. Yuan et al. [19] conducted an experimental investigation on OTEC system using ammonia-water as working fluid. Effects of heating and cooling source temperature, as well as the solution flow rate on system performance were investigated, the results show that heating source temperature contributes the most significant effects.

Although many studies have investigated thermodynamic optimization of OTEC systems, in which maximum thermal efficiency is usually selected as objective function. It should be stressed that the maximization of cycle efficiency is not a reasonable optimization objective in an OTEC plant, although the thermal energy contained in ocean is nearly inexhaustible. The maximum cycle efficiency usually refers to high evaporating and low condensing temperature for a Rankine cycle, however, to pursue maximum efficiency would lead to a reduction of heat recovery rate of seawater which has variable temperature. It should be stressed at this point that in some cases, increase of cycle power output is more important than how efficient a thermodynamic cycle is. OTEC cycle utilizes a major portion of net power for pumping the seawater. Since the seawater is pumped up, heat/cold energy carried by seawater should be entirely utilized, just like it is done in a geothermal power plant. A proper objective function called specific net power output is selected to evaluate power cycle performance [20]. As discussed in [3], the best theoretical power cycle for OTEC is a Lorenz cycle. Lorenz cycle refers to an ideal trapezoidal cycle if a limit in reinjection temperature is considered. Lorenz cycle has variable temperature during heating and cooling processes, and it is suitable for variable temperature heat source/sink (warm seawater with temperature decrease and cold seawater with temperature increase). Given this, Lorenz cycle enables entire work availability utilization of seawater. It has been proved that a Lorenz cycle produces larger specific work than Carnot cycle or multi-cycle [3].

In the above context, this work aims to explore the optimized thermodynamic performance of closed off-shore OTEC system based on Rankine cycle. In order to approach the ideal Lorenz cycle, Rankine cycle using CO_2-based binary zeotropic mixtures are novelty proposed for OTEC application. It is noteworthy that CO_2-rich mixtures exhibit good properties in safety and environmental impact, and they have been proven to be effective working fluids in many other applications [21,22]. To the authors' best knowledge, there has not been any published work in OTEC power cycle using CO_2-based binary mixture. Pure working fluids, including NH_3 and CO_2, are also comparatively investigated with mixtures. Different effects on cycle performance are analyzed. Overall optimization to maximize the system thermal efficiency and specific work to warm seawater flow rate are carried out, respectively. A preliminary economic analysis using the ratio of net power output to total heat transfer area is also conducted. This work may contribute to OTEC cycle design and application of novel CO_2-based binary mixtures. In addition, the optimized data may serve as future reference.

2. Methodology

2.1. Description of the OTEC system

Basically, an OTEC system consists of a working fluid pump, an evaporator, a turbine, a generator, a condenser, and pumps for both warm and cold seawater, as shown in Fig. 1. The Rankine cycle consists of four processes: the saturated liquid is first compressed to high pressure (1–2), it then flows into the evaporator and receives heat from warm surface seawater, being vaporized at the outlet (2–3). Afterwards, the high-pressure vapor flows into the turbine and its enthalpy drop is converted into work (3–4). Finally the low pressure vapor flows into the condenser and is liquefied by cold deep seawater (4–1). The water pump circulates seawater into exchangers to exchange heat with working fluid.

The *T-s* diagram of a Rankine cycle is shown in Fig. 2, using pure working fluid and CO_2-based binary mixture, respectively. Seawater is sensible heat source of finite heat capacity, and its temperature changes during a heat transfer process. As shown in Fig. 2a, pure working fluid has isothermal evaporating and condensing process. During heat addition process, the latent heat of fluid is dominant in amount.. To avoid intersection of temperature profiles during heat transfer, a limit of pinch point temperature difference must be imposed. Due to this limit, the entrance and terminal temperature difference in evaporator is relatively larger than pinch temperature difference. Turbine inlet temperature of working fluid and outlet temperature of warm seawater are both restricted, resulting in decreasing of both cycle thermal efficiency and heat addition. The pinch point locates at cold seawater outlet in condensing process, and condensing temperature is restricted by cold seawater inlet temperature and its temperature rise. The entrance temperature difference in condenser is relatively larger. Therefore, a Rankine cycle using pure working fluid does not match well with warm/cold seawater.

In order to increase the utilization of sensible heat source/sink, CO_2-based binary zeotropic mixtures are considered as working fluid. As shown in Fig. 2b, the temperature glide in evaporating/condensing process improves thermal match. The pinch point appears inside condensing process, and more temperature lift for cold seawater could be achieved. Temperature profiles along the heat exchanger are nearly parallel, and terminal temperature difference of heat exchangers (outlet of both evaporator and condenser) could be equal to pinch point temperature difference. Thus the irreversibility could be minimized during heat transfer process.

The analysis is based on the first-law of thermodynamics. Parametric optimization and discussion are performed to maximize Rankine cycle thermal efficiency, OTEC system thermal efficiency, and net power output per unit mass flow rate of warm seawater, respectively. The basic equations of energy analysis for OTEC system are expressed as follows.

Heat input in evaporator:

$$\dot{Q}_{in}=\dot{m}_{wf}(h_3-h_2)=\dot{m}_{ws}c_{p,ws}(T_{ws,in}-T_{ws,out}) \tag{1}$$

Heat rejection in condenser:

$$\dot{Q}_{out}=\dot{m}_{wf}(h_4-h_1)=\dot{m}_{cs}c_{p,cs}(T_{cs,out}-T_{cs,in}) \tag{2}$$

Working fluid pump power consumption:

$$\dot{W}_p=\dot{m}_{wf}(h_2-h_1) \tag{3}$$

Turbine power output:

$$\dot{W}_t=\dot{m}_{wf}(h_3-h_4) \tag{4}$$

The pump and turbine isentropic efficiency can be expressed as:

$$\eta_p=(h_{2s}-h_1)/(h_2-h_1) \tag{5}$$

$$\eta_t=(h_3-h_4)/(h_3-h_{4s}) \tag{6}$$

Power output and thermal efficiency of Rankine cycle:

$$\dot{W}_{cycle}=\dot{W}_t-\dot{W}_p \tag{7}$$

$$\eta_{cycle}=\frac{\dot{W}_{cycle}}{\dot{Q}_{in}} \tag{8}$$

In view of the low efficiency of Rankine cycle and fairly long distance for sea water transport, the effect of the water pump power consumption on OTEC system cannot be neglected. The power consumption of seawater pump is expressed as follows.

$$\dot{W}_{p,ws(cs)}=\frac{\dot{m}_{ws(cs)}\Delta p_{ws(cs)}}{\rho_{ws(cs)}\eta_{p,ws(cs)}} \tag{9}$$

where $\dot{W}_{p,ws}$ and $\dot{W}_{p,cs}$ are the power consumptions of warm seawater pump and cold seawater pump, respectively. $\Delta p_{ws(cs)}$ is the total pressure drop along seawater pipeline.

For the warm seawater piping, the total pressure dop can be defined as [7]:

$$\Delta p_{ws}=(\Delta p_{ws})_P+(\Delta p_{ws})_E \tag{10}$$

where $(\Delta p_{ws})_P$ is the pressure drop of the warm seawater pipe, expressed as:

$$(\Delta p_{ws})_P=(\Delta p_{ws})_{SP}+(\Delta p_{ws})_B \tag{11}$$

where $(\Delta p_{ws})_{SP}$ is the friction loss of the straight pipe and $(\Delta p_{ws})_B$ is the

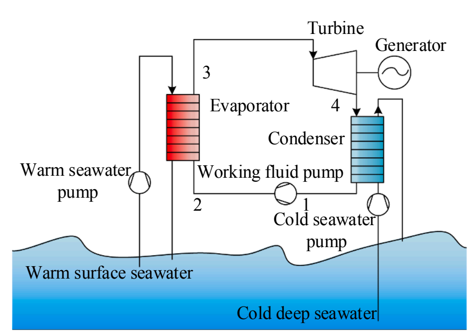

Fig. 1. The schematic diagram of an OTEC system.

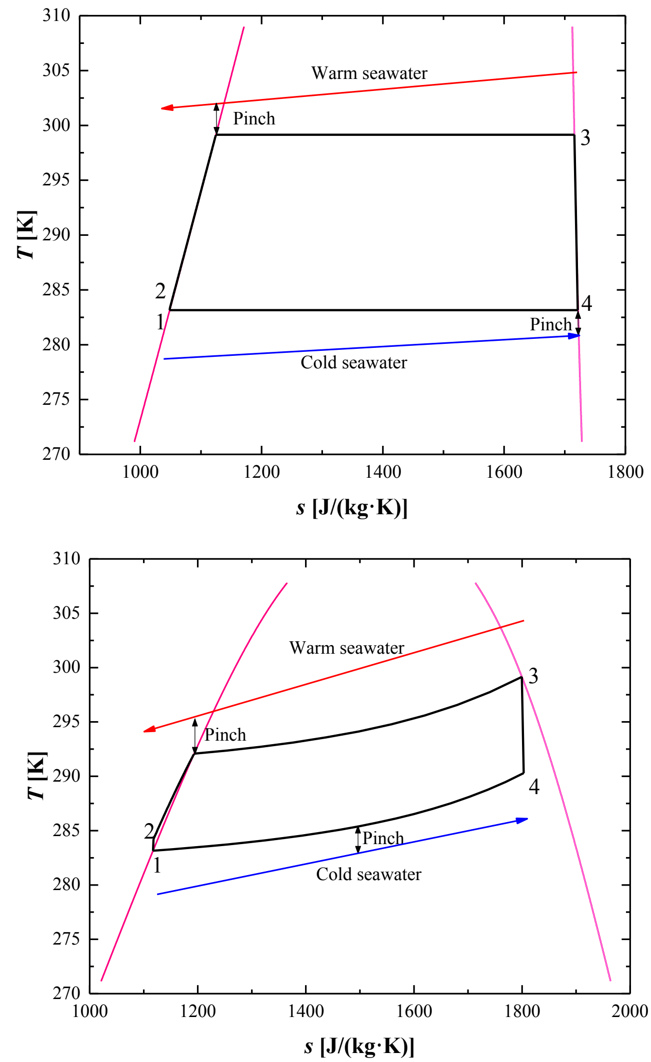

(a) Pure working fluid (b) CO2-based binary mixture

Fig. 2. *T-s* diagram of Rankine cycle.

bending loss alone the warm seawater pipe. $(\Delta p_{ws})_{SP}$ can be expressed as:

$$(\Delta p_{ws})_{SP}=f\frac{\rho_{ws}L_{ws}v_{ws}^2}{2D_e} \tag{12}$$

where f represents the fanning friction factor, and f can be expressed by Colebrook-White equation [23]:

$$\frac{1}{\sqrt{f}}=-2\log\left(\frac{2.51}{Re\sqrt{f}}+\frac{K/D_e}{3.72}\right) \tag{13}$$

where K is the pipeline absolute roughness, Re is Reynolds Number.

$(\Delta p_{ws})_B$ can be expressed as [7]:

$$(\Delta p_{ws})_B=(f_I+f_V+f_S+f_J+f_O+f_e+f_d+f_r)\rho_{ws}v_{ws}^2/2=f_B\rho_{ws}v_{ws}^2/2 \tag{14}$$

where f_I is the inlet loss coefficient, f_V is the valve loss coefficient, f_S is the separating loss coefficient, f_J is the joint loss coefficient, f_O is the outlet loss coefficient, is the elbow loss coefficient, f_d is the diffuser loss cofficient, f_r is the reducer loss coefficient.

$(\Delta p_{ws})_E$ represents the pressure drop of the warm seawater in plate-type evaporator:

$$(\Delta p_{ws})_E=(\Delta p_{ws})_{FE}+(\Delta p_{ws})_{ME}+(\Delta p_{ws})_{GE} \tag{15}$$

where $(\Delta p_{ws})_{FE}$ is the frictional pressure drop, $(\Delta p_{ws})_{ME}$ is the pressure loss at the inlet and outlet, and $(\Delta p_{ws})_{GE}$ is the gravitation pressure drop in evaporator [24].

The pressure loss at inlet and outlet can be expressured by

$$(\Delta p_{ws})_{ME}=1.5\rho_{ws}v_{ws}^2/2 \tag{18}$$

Frictional pressure drop can be expressured by:

$$(\Delta p_{ws})_{FE}=4f\frac{\rho_{ws}L_E v_E^2}{2D_E} \tag{19}$$

where f is the friction factor in evaporator, L_E is the length of path, D_E is the hydaulic diameter, defined as:

$$D_E=\frac{2wb_c}{w+b_c} \tag{20}$$

where w is the plate width inside gasket, and b_c is the mean spacing between the plates.

For a plate heat exchanger with chevron angles of 60°, the friction factor can be calculated by [24]:

$$f=2.48Re^{-0.20} \tag{21}$$

For the cold seawater piping, the total pressure dop can be defined as:

$$\Delta p_{cs}=(\Delta p_{cs})_P+(\Delta p_{cs})_C+(\Delta p_{cs})_d \tag{22}$$

where $(\Delta p_{cs})_P$ is the pressure of the cold seawater pipe, $(\Delta p_{cs})_C$ is the pressure of cold seawater in condenser, the calculation is similar to that of warm seawater. $(\Delta p_{cs})_d$ represents the pressure difference caused by the density difference between warm and cold seawater, defined as [7]:

$$(\Delta p_{cs})_d=L_{cs}\rho_{cs}\left(1-\frac{\rho_{ws}+\rho_{cs}}{2\rho_{cs}}\right)g \tag{23}$$

The totale net power output of an OTEC system is expressed as:

$$\dot{W}_{net}=\dot{W}_t-\dot{W}_p-\dot{W}_{p,ws}-\dot{W}_{p,cs} \tag{24}$$

The system thermal efficiency of OTEC can be determined as:

$$\eta_{sys}=\frac{\dot{W}_{net}}{\dot{Q}_{in}} \tag{25}$$

In order to objectively compare various cycle designs with different workings fluids, the specific net power output is used. The specific net power output is defined as the net power output per unit mass flow rate of warm seawater, and it can be determined as follows [20]:

$$w_{net,spec}=\frac{\dot{W}_{net}}{\dot{m}_{ws}}\quad [\mathrm{kJ/kg}] \tag{26}$$

The ratio between net power output and heat exchangers area is used for a preliminary economic analysis, γ defined as:

$$\gamma=\frac{\dot{W}_{net}}{A_{tot}} \tag{27}$$

The detailed mathematical models of the heat exchangers are depicted in Appendix A.

The pinch point temperature difference in heat exchanger is an important parameter to be calculated as constraint, which is calculated by an element division and iteration method in [25]. For each iteration, the heat exchange length is discretized into 100 segments and the temperature difference is checked.

Table 1
Properties of working fluids [30].

Working fluid	T_c (°C)	p_c (MPa)	Molar mass (g/mol)	ODP	GWP	Safety
CO_2	31.1	7.38	44.01	0	1	A1
R32	78.1	5.78	52.02	0	675	A2
R1234yf	94.7	3.38	114.04	0	< 4.4	A2L
R134a	101.1	4.06	102.03	0	1370	A1
R161	102.2	5.09	48.06	0	12	A3
R1234ze(E)	109.4	3.64	114.04	0	6	A2L
R152a	113.3	4.52	66.05	0	124	A2
NH_3	132.3	11.33	17.03	0	< 1	B2

2.2. Selection of working fluids

Working fluid selection is a key aspect for Rankine cycle optimization, and the most important criteria for the selection of working fluid is good thermodynamic performance. Besides, transport, safety and environmental properties are also important aspects in working fluid selection. CO_2 has advantages in use as working fluid such as zero ODP, low GWP, non-explosive, non-flammable, non-toxic, stable and relative inert, abundant and low cost, etc. In view of the moderate critical pressure and low critical temperature, CO_2 has potential in low-grade heat resource recovery [26], and various cycle configurations have been widely investigated. In order to ensure that the actual cycle serves close to an ideal Lorenz cycle, CO_2-based binary zeotropic mixtures are considered to be working fluids. The second component of mixture is suggested to be zero-ODP, low-GWP, nonflammable and non-reactive with CO_2. After an initial screening, six working fluids were selected as potential as potential additives into CO_2 as listed in Table 1. Among them, R32 is flammable, and R134a is with high GWP, etc. Nonetheless, their mixtures with high CO_2 concentration are considered to be non-flammable, safe [27] and environmental-friendly [21,28] working fluids. The properties of the mixtures are based on REFPROP 9.0 [29].

Fig. 3 shows the temperature glide of six mixtures with variation of CO_2 mass fraction at a fixed saturated vapor temperature of 28 °C. As the figure illustrated, temperature glide of a certain mixture changes with mass fraction of CO_2, and there exists a maximum value. Besides, the variation tendency of temperature glide differs among different mixtures. Considering the low temperature difference between hot and cold sources, a temperature glide of no larger than 10 °C may be appropriate to guarantee the feasibility of power cycle. To ensure the stability of OTEC system, the gradient of temperature glide should be smooth. The working pairs of CO_2/R32, CO_2/R1234yf seems to be potential candidates.

2.3. Assumption of the analysis

The simulation conditions used in this study are listed in Table 2. The constant parameters (e.g. component efficiency, length of seawater pipe, etc.) are assumed to be fixed. The boundaries of decision variables (e.g. evaporating and condensing temperature, etc.) are restricted by environmental condition and pinch limit. The dependent variables (e.g. outlet temperature of warm and cold seawater, mass flow rate of fluid, etc.) are based on the energy balance, and affected by other parameters. The surface seawater normally has a temperature range of 24–30 °C [9,31] in summer season, and it is considered to be external variable. In this project, fixed heat input for Rankine cycle, rather than fixed mass flow rate of warm seawater, is assumed. The mass flow rate of seawater is determined by its temperature variation among heat rejection. The total net power output is the product of system efficiency and heat supplied to cycle, therefore, it is corresponding to OTEC system thermal efficiency.

A Matlab program is designed for the simulation, and a flow chart for the simulation is listed in Appendix B. As shown in Fig. A.1, optimization is carried out using “Direct Search method”. The basic idea is to simplify the multi-dimensional optimization by using a series of one-dimensional searches to find the optimum. The pinch point location is calculated by an element division and iteration method. The iteration stops when the difference between the calculated $\triangle T_{pp,\ cal}$ with the default $\triangle T_{pp,\ set}$ is < 0.0001 °C. The assumptions ensure enough accuracy of results.

To facilitate the simulation, the following assumptions and simplifications are formulated in this project:

1) Each component of OTEC system is considered to be steady-state and steady-flow.
2) The kinetic and potential energies, friction and pressure losses of working fluid are neglected.
3) Heat exchange (heat losses of hot fluid, and heat gains in the cool water pipeline) with the surroundings are negligible.
4) Overall composition of mixture in each component keeps constant.
5) The leakage of working fluid from the components are negligible.

3. Results and discussion

3.1. Influence of working fluid composition

Composition is a key factor that influences the property of mixture as well as its cycle performance. Fig. 4 illustrates the variation of Rankine cycle efficiency with CO_2 mass fraction for different mixtures. The saturated liquid temperature in condensing ($T_{cond,\ l}$) and saturated vapor temperature in evaporating ($T_{evap,\ g}$) are fixed, It is interesting to note that thermal efficiency varies in a counter direction to the mixture temperature glide, and pure CO_2 outputs the maximum efficiency. This is mainly because the temperature glide during evaporating/condensing process induces the increasing of mean heat rejection temperature and decreasing of mean heat addition temperature. Thus, temperature glide is disadvantaged to improve cycle thermal efficiency, in other words, pure fluid is a better choice for maximization of thermal efficiency.

Fig. 5 shows the variation of Rankine cycle and OTEC system thermal efficiency with CO_2 mass fraction, taking CO_2/R32 mixture for example. There exists two local maximum value for both η_{cycle} and η_{sys}.

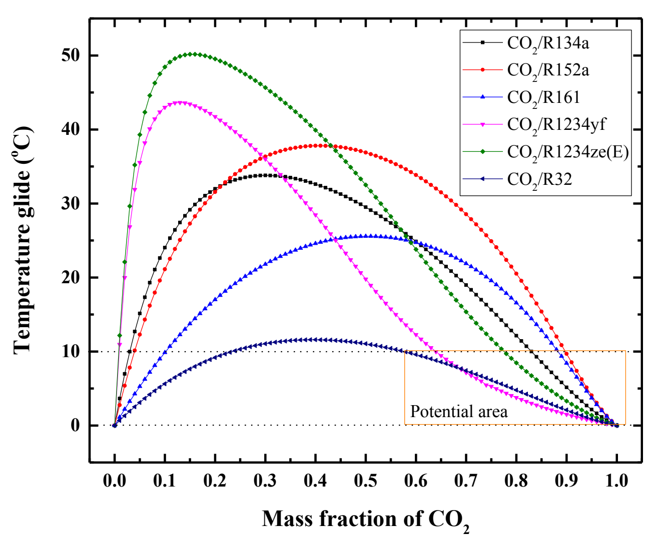

Fig. 3. Temperature glide variation of different binary mixtures.

Table 2
Specifications of the model.

Parameter	Value
Heat input of OTEC, $\dot{Q}_{in}$ (MW)	1
Warm seawater inlet temperature, $T_{ws,\ in}$ (°C)	26–30 [9]
Deep cold seawater inlet temperature, $T_{cs,\ in}$ (°C)	5 [12]
Pinch point temperature difference, ΔT_{pp} (°C)	2 [6,32]
Turbine efficiency, η_t	85% [33]
Working fluid pump efficiency, η_p	80% [13,34]
Seawater pump efficiency, $\eta_{p,\ ws(cs)}$	80% [7,35]
Roughness of seawater pipeline, K (μm)	4 [35]
Seawater velocity in pipeline, v (m/s)	1 [3,36]
Length of warm seawater pipeline, (m)	200 [3]
Length of cold seawater pipeline, (m)	1000 [7,32]

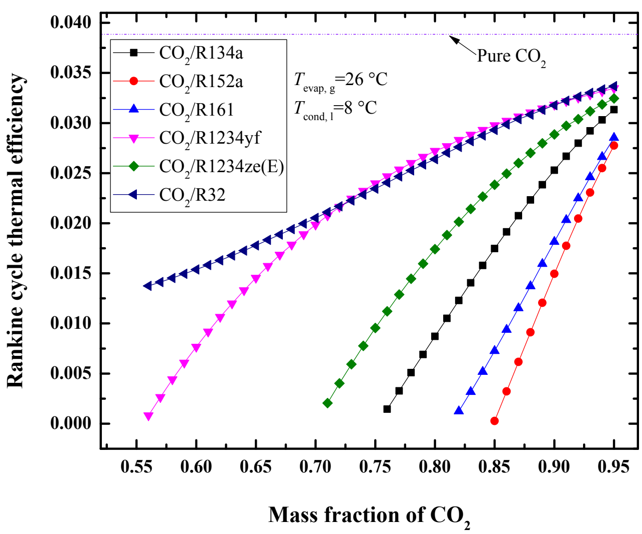

Fig. 4. Variation of Rankine cycle thermal efficiency with mass fraction of CO_2.

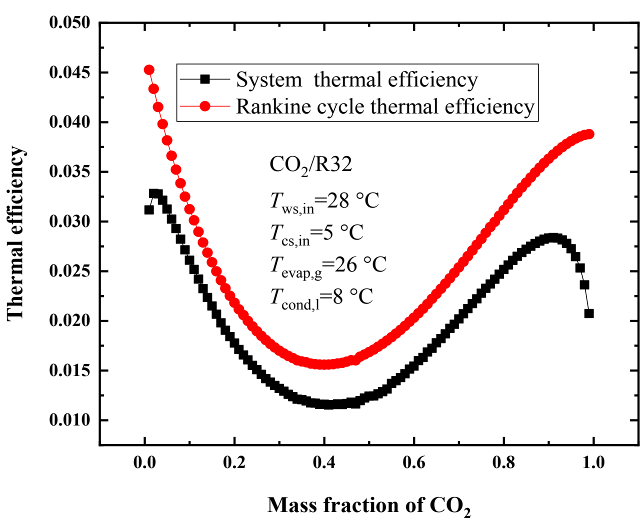

Fig. 5. Variation of Rankine cycle and OTEC system thermal efficiency with CO_2 mass fraction.

Rankine cycle efficiency achieves the maximum value in case of using pure fluid. While for system efficiency, the seawater pump power consumption plays an important role, with an efficiency penalty of about 0.5% to 1%. The local maximum values for η_{sys} are obtained at x_{CO_2} = 0.02, x_{CO_2} = 0.91, respectively. This is mainly due to that mixture's temperature glide improves thermal matching between working fluid and seawater. It allows a lager temperature difference between

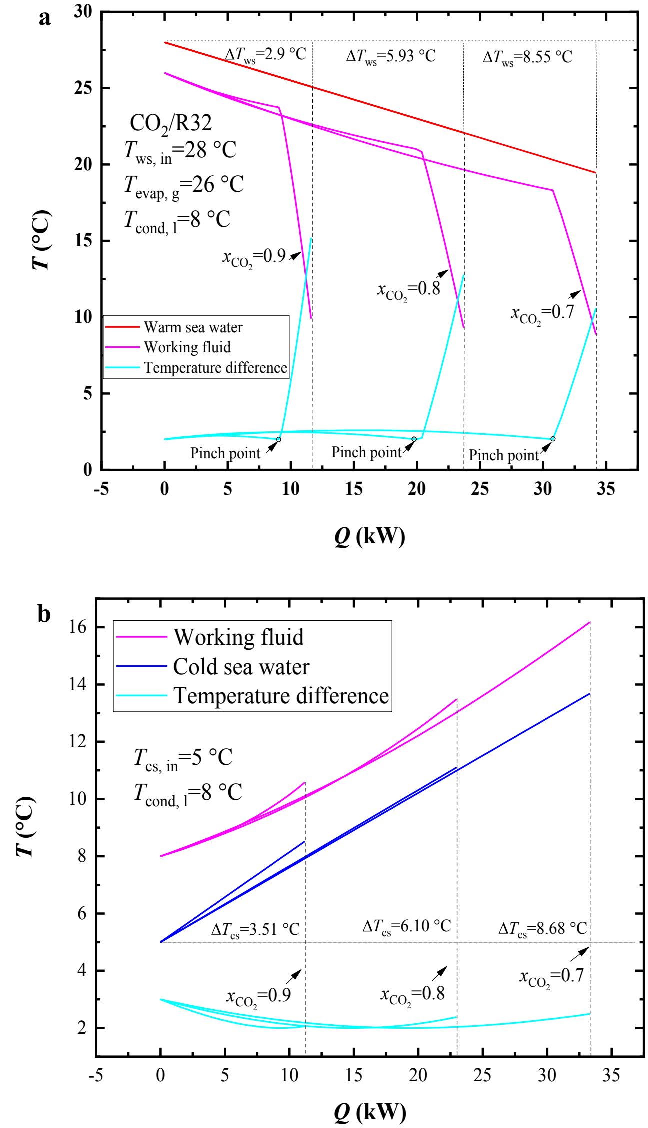

Fig. 6. Temperature profile matches between OTEC working fluid and external fluids (a. warm seawater; b. cold seawater).

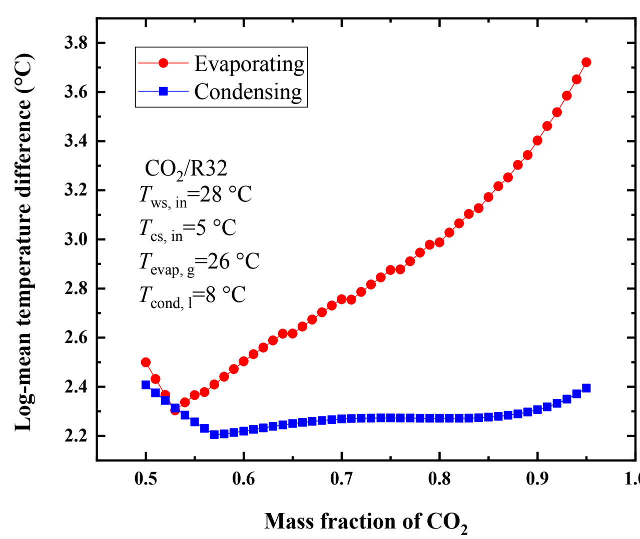

Fig. 7. Effect of mass fraction of CO_2 on log-mean temperature difference in evaporating and condensing process.

inlet and outlet of seawater, thus, a smaller mass flow rate of seawater is needed at given exchanging heat quantity. Power consumption of seawater pump decreases with increasing of mixture's temperature glide. The optimal value of η_{sys} is obtained after comprehensive consideration of seawater pump power consumption and cycle thermal efficiency variation with x_{CO_2}.

Fig. 6 illustrates temperature profiles and pinch locations between working fluid and external fluids at different CO_2 concentration. Mass flow rate of warm seawater is set to be 1 kg/s, and mass flow rate of cold seawater is calculated dependently based on energy balance. As shown in Fig. 6a, thermal matching improves as mass fraction of CO_2 decreases from 0.9 to 0.7, resulting in a larger heat input from a certain flow rate of heat source. Temperature difference between warm seawater inlet and outlet (ΔT_{ws}) is calculated to be 2.9, 5.93 and 8.55 °C at x_{CO_2} = 0.9, 0.8 and 0.7, respectively. Therefore, in the case of same heat source mass flow, the heat received for OTEC with x_{CO_2} = 0.7 is nearly three times as much as that with x_{CO_2} = 0.9. With the proper increase of temperature glide, a larger ratio of latent heat transfer to overall heat transfer is achieved, and a lower mean temperature difference along evaporator is obtained. As shown in Fig. 7, the log-mean temperature difference achieves the minimum value of 2.3 °C at x_{CO_2} = 0.53. Similar results for condenser could also be obtained, as shown in Fig. 6b. ΔT_{cs} is calculated to be 3.51, 6.1 and 8.68 °C at x_{CO_2} = 0.9, 0.8 and 0.7, respectively. Temperature profiles of working fluid and cold seawater are nearly parallel, and heat transfer temperature difference along the path is rather closed to pinch point temperature difference. The minimum log-mean temperature difference of 2.2 °C is obtained at x_{CO_2} = 0.57. The above analyses indicate that temperature glide of mixture makes Rankine cycle serve like Lorenz cycle. Zeotropic mixture with adequate temperature glide can enhance the utilization of sensitive heat source/sink.

In the condition of fixed heat input of 1 MW for OTEC system, the influence of CO_2 concentration on mass flow rate and corresponding temperature variation of seawater is illustrated in Fig. 8. Temperature difference between seawater inlet and outlet varies in a counter direction to the mass fraction of CO_2, and increasing mass flow rate of seawater is needed to guarantee the formulated heat input. With the increasing of CO_2 mass fraction, mass flow rate of seawater initially increases modestly and then sharply due to changes of working fluid's temperature glide. Note that seawater pumping power is closed related to the mass flow rate of seawater, and plays a significant role in the determination of net power in an OTEC system.

Fig. 9 illustrates the variation of system specific net power output ($w_{net,\ spec}$) with CO_2 mass fraction. It should be noted that the maximum $w_{net,\ spec}$ is equal to the maximization of system net power output under given mass flow rate of warm water. Furthermore, the maximum $w_{net,\ spec}$ indicates the minimum seawater flow rate to produce the same power output for OTEC system, thus, the diameter of pipe and exchanger size could be reduced. As shown in the figure, there exists an optimal value of CO_2 mass fraction for each mixture to produce the maximum $w_{net,\ spec}$. The optimum values differ from each other, mainly ranging from about 678 to 693 J/kg under survey conditions. The maximum specific power output is obtained when cycle efficiency, heat recovery rate of seawater and thermal matching between cycle and heat source/sink are synthetically considered. While the temperature glide has great effects on above mentioned factors. According to Fig. 3, the optimal value is obtained when evaporating temperature glide is about 8 °C under this case study.

3.2. Influence of evaporating and condensing temperature

Fig. 10 shows the influence of evaporating temperature (saturated vapor temperature for mixture) on OTEC system efficiency and specific net power output. Mixtures as well as pure fluid of CO_2 and NH_3 are investigated, while the mass fraction of CO_2 is fixed at 0.9 for each mixture. As the figure shows in this case study, OTEC system thermal efficiency is strongly linearly related to evaporating temperature. As evaporating temperature increases from 20 to 26 °C, system efficiency increases about 67.8% taking CO_2/R32 for example. Mixtures of CO_2/R32 and CO_2/R1234yf achieve a higher system efficiency at evaporating temperature below 24 °C, otherwise, NH_3 produces a higher system efficiency. With respect to the specific net power output, most mixtures have an optimum evaporating temperature, while CO_2/R152a and CO_2/R161 achieve progressive increase with the evaporating temperature. The optimum evaporating temperature is related to temperature glide, and a proper larger value of temperature glide results in an increasing value of optimum evaporating temperature. It can be found that optimum values for mixtures are higher than the values for pure working fluids. In view of the improved coupling of power cycle and heat source, mixtures produce significant larger specific net power output than the pure working fluids.

Fig. 11 illustrates the effects of condensing temperature (saturated liquid temperature for mixture) on OTEC system efficiency and specific net power output. The system efficiency and specific net power output of mixtures decrease linearly with the increase of condensing temperature, while for the pure working fluid, the slop first increases sharply and then becomes flat. This is mainly due to the reason that the cold seawater pump power consumption is largely dependent on the mass flow rate of cold seawater, while the mass flow rate of cold seawater is mainly determined by temperature rise of seawater. For the pure working fluid, the outlet temperature of cold seawater is equal to the difference value between condensing temperature and pinch temperature difference, thus, the temperature rise is restricted by condensing temperature. As the condensing temperature moves downwards, the cold seawater mass flow rate will increase sharply, and this induces more pump power consumption in turn. The initial increase of η_{sys} or $w_{net,\ spec}$ is mainly due to the reduction of seawater pump power, however, the further increase of condensing temperature will lead to the decline of Rankine cycle efficiency. For the mixtures, the temperature glide allows a lager temperature rise of cold seawater, and variation of cold seawater mass flow rate with $T_{cond,\ l}$ is unapparent. Thus, the influence from cold seawater pump power is minor. The linear decrease of η_{sys} or $w_{net,\ spec}$ is mainly due to the decline of Rankine cycle efficiency.

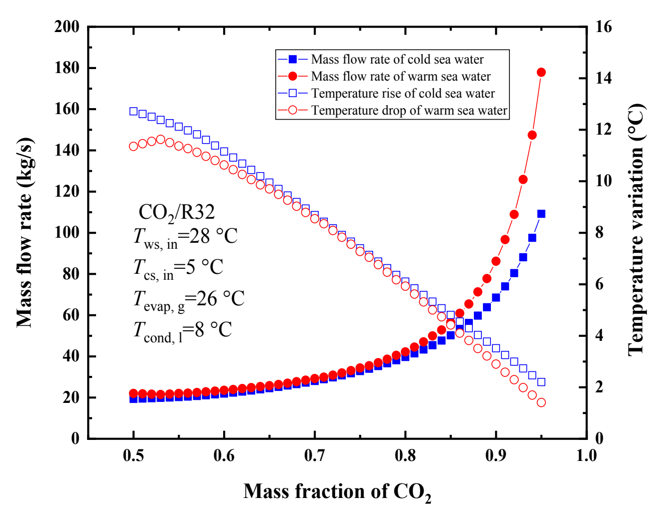

Fig. 8. Influence of CO_2 concentration on seawater mass flow rate and corresponding temperature variation.

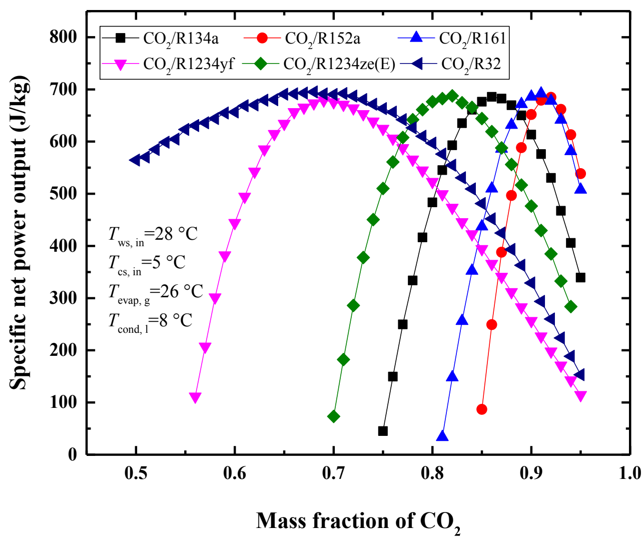

Fig. 9. Variation of system specific net power output with CO_2 mass fraction.

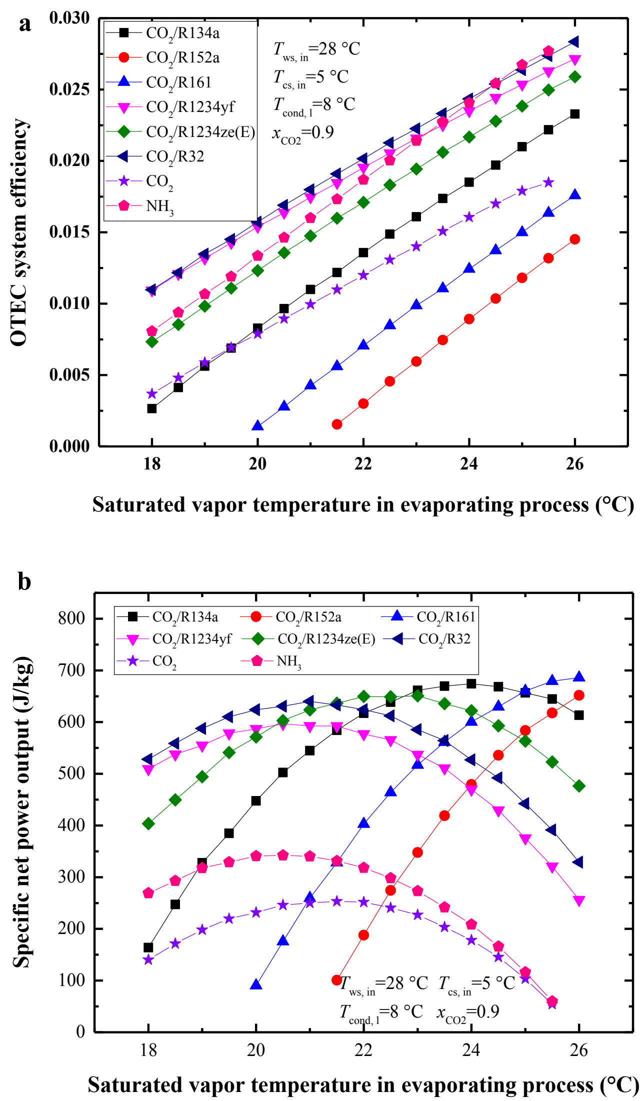

Fig. 10. Effects of evaporating temperature on system performance (a. system thermal efficiency; b. specific net power output).

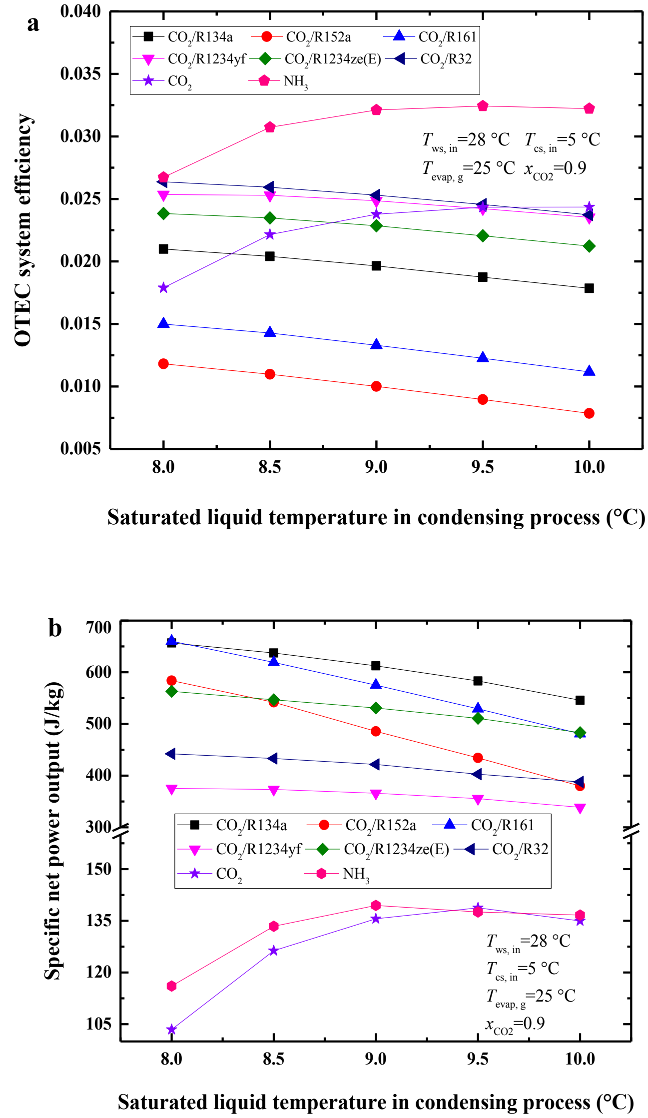

Fig. 11. Effects of condensing temperature on system performance (a. system thermal efficiency; b. specific net power output).

3.3. Influence of warm seawater temperature

Higher warm seawater temperatures and lower cold seawater temperatures increase the net output power and efficiency of an OTEC system. The surface warm seawater temperature is affected by weather, daytime cycle and season, thus effects of warm seawater temperature ranging from 26 to 28 °C on system thermal efficiency and specific net power output are illustrated in Fig. 12. Both system thermal efficiency and specific net power output increase almost linearly for each working fluid with $T_{ws,\ in}$ ranging from 26 to 28 °C. A variation of 1 °C in the warm seawater resource corresponds to a change in system efficiency of about 8%, yet a change in specific net power output of the order of about 15%, taking CO_2/R32 into consideration.

3.4. Optimum cycle design for each working fluid

For an OTEC system with heat input of 1 MW, the overall optimum system configurations at maximum system efficiency and specific net power output for different working fluid are obtained, as listed in Table 3 and Table 4, respectively. As the results indicate, the optimum cycle design under different optimization objective differs largely from

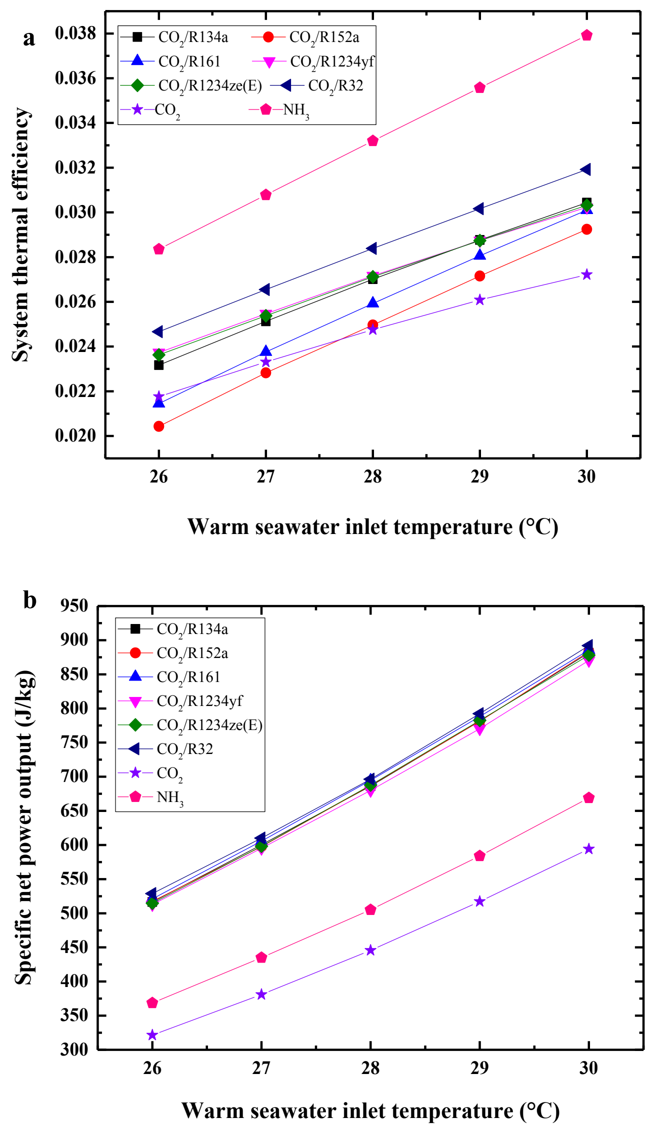

Fig. 12. Effects of warm seawater temperature on system performance (a. system thermal efficiency; b. specific net power output).

each other. For the maximization of system efficiency, NH_3 produces the maximum value of 3.32%, and CO_2/R32 (0.91/0.09 wt%) produces the maximum of 2.84% among the mixtures. Although pure CO_2 generates the maximum turbine power of 52.88 kW, it also consumes the highest working fluid pump of 17.93 kW, thus it outputs the lowest system efficiency of 2.48%. The mixtures have lower working pump power than pure CO_2, owning to the reduction of pressure difference between evaporating and condensing process. In view of the low press difference of 0.21 MPa, NH_3 has a negligible working pump power of only 0.67 kW.

For the maximization of specific net power output, the mixtures produce significant higher net power than the pure working fluid. CO_2/R32 (0.76/0.24 wt%) outputs the maximum value of 0.696 kJ/kg, however, the optimum values of other mixtures are also very close to that of CO_2/R32. This is mainly because the temperature glide of mixture could be adjusted by changing composition, each mixture cold achieve optimal coupling with heat source/sink. Temperature change of heat source/sink varies among mixtures, and it is higher than that of pure working fluids. Therefore, the heat source/sink supplies more heat/cold energy to the mixtures. For the pure working fluids, the only way to increases utilization of warm seawater is to reduce its evaporating temperature. The optimized evaporating temperature is only 19 °C for NH_3, resulting in larger heat transfer irreversibility and a lower $w_{net,spec}$ value of 0.505 kJ/kg The optimum system design under maximum specific net power is obtained after making a proper compromise between cycle efficiency and heat input.

3.5. Preliminary economic analysis

Since the heat exchanger cost is one of the major costs of OTEC plant [7], the ratio between net power output and heat exchangers area is suggested to be the metric for preliminary economic analysis of OTEC system [3,7,12]. Therefore, effects on γ for different working fluids are comparatively analyzed.

Fig. 13 illustrates the effects of CO_2 mass fraction on γ. The value of γ first increases and then decreases with increasing CO_2 mass fraction for CO_2/R134a, CO_2/R1234yf and CO_2/R32 under survey conditions. For other mixtures, the value of γ increases with increasing CO_2 mass fraction. The optimal values for different mixtures are very close to each other. Among the mixtures, CO_2/R32 produces the maximum value of 62.78 W/m^2 at CO_2 mass fraction of 0.86.

The effects of evaporating and condensing temperature on γ are illustrated in Fig. 14 and Fig. 15, respectively. CO_2 mass fraction of 0.9 is

Table 3
System configurations under maximum system efficiency.

Parameters	M1	M2	M3	M4	M5	M6	NH_3	CO_2
Mass fraction of CO_2	0.95	0.95	0.95	0.89	0.94	0.91	–	–
Evaporating temperature, °C	26	26	26	26	26	26	25.5	25.5
Evaporating temperature glide, °C	2.4	4.4	4.0	1.9	2.0	2.0	–	–
Evaporating pressure, MPa	6.00	5.62	5.61	5.93	6.06	5.81	1.02	6.51
Condensing temperature, °C	8.0	8.0	8.0	8.0	8.0	8.0	9.5	9.5
Condensing temperature glide, °C	3.8	6.1	5.5	3.0	3.1	3.0	–	–
Condensing pressure, MPa	4.15	4.08	4.03	4.07	4.15	3.98	0.81	4.45
Mass flow rate of warm seawater, kg/s	79.59	46.37	51.06	96.12	95.57	96.68	462.76	344.68
Temperature drop of warm seawater, °C	3.14	5.39	4.90	2.60	2.62	2.59	0.54	0.73
Mass flow rate of cold seawater, kg/s	80.82	59.42	57.34	80.14	86.42	73.97	95.56	96.46
Temperature rise of cold seawater, °C	2.98	4.07	4.21	3.01	2.79	3.25	2.5	2.5
Power generation of turbine, kW	49.74	43.15	44.08	51.30	51.26	49.82	44.66	52.88
Working fluid pump power, kW	13.87	10.72	10.89	15.41	14.94	13.08	0.67	17.93
Seawater pump power, kW	8.86	7.46	7.27	8.72	9.20	8.34	10.79	10.19
System net power output, kW	27.01	27.97	25.93	27.17	27.12	28.39	33.20	24.76
System thermal efficiency, %	2.70	2.80	2.59	2.72	2.71	2.84	3.32	2.48
Specific net power output, kJ/kg	0.339	0.538	0.507	0.283	0.283	0.294	0.072	0.072

M1: CO_2/R134a, M2: CO_2/R152a, M3: CO_2/R161, M4: CO_2/R1234yf, M5: CO_2/R1234ze(E), M6: CO_2/R32.

Table 4
System configurations under maximum specific net power output.

Parameters	M1	M2	M3	M4	M5	M6	NH_3	CO_2
Mass fraction of CO_2	0.86	0.92	0.91	0.72	0.83	0.76	–	–
Evaporating temperature, °C	25.5	25.5	25.5	25.0	25.5	24.5	19	20
Evaporating temperature glide, °C	8.4	7.9	7.9	7.1	7.3	6.3	–	–
Evaporating pressure, MPa	4.84	4.97	4.82	4.65	4.93	4.46	0.83	5.73
Condensing temperature, °C	8	8	8	8	8	8	9.5	9.5
Condensing temperature glide, °C	3.8	6.1	5.5	3.0	3.1	3.0	–	–
Condensing pressure, MPa	3.91	3.97	3.85	3.69	3.88	3.50	0.60	4.45
Mass flow rate of warm seawater, kg/s	24.80	26.19	26.27	26.82	27.75	28.34	34.29	34.22
Temperature drop of warm seawater, °C	10.08	9.55	9.52	9.32	9.01	8.82	7.29	7.31
Mass flow rate of cold seawater, kg/s	37.52	41.59	36.55	35.94	39.46	33.72	97.28	97.46
Temperature rise of cold seawater, °C	6.51	5.87	6.68	6.79	6.18	7.23	2.5	2.5
Power generation of turbine, kW	28.75	30.51	30.02	31.35	32.34	20.83	27.40	35.43
Working fluid pump power, kW	6.07	6.47	6.10	7.57	7.40	5.70	0.37	10.17
Seawater pump power, kW	5.66	6.04	5.67	5.54	5.85	5.39	9.72	10.01
System net power output, kW	17.02	18.00	18.25	18.24	19.08	19.74	17.32	15.25
System thermal efficiency, %	1.70	1.80	1.83	1.82	1.91	1.97	1.73	1.53
Specific net power output, kJ/kg	0.686	0.687	0.695	0.680	0.688	0.696	0.505	0.446

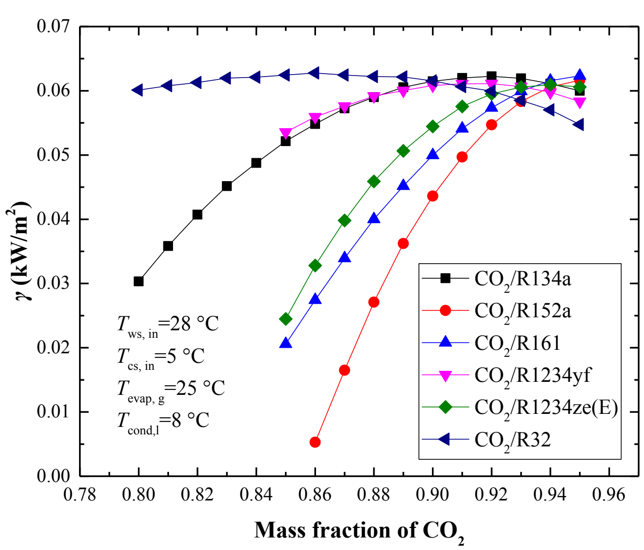

Fig. 13. Effects of mass fraction of CO_2 on γ.

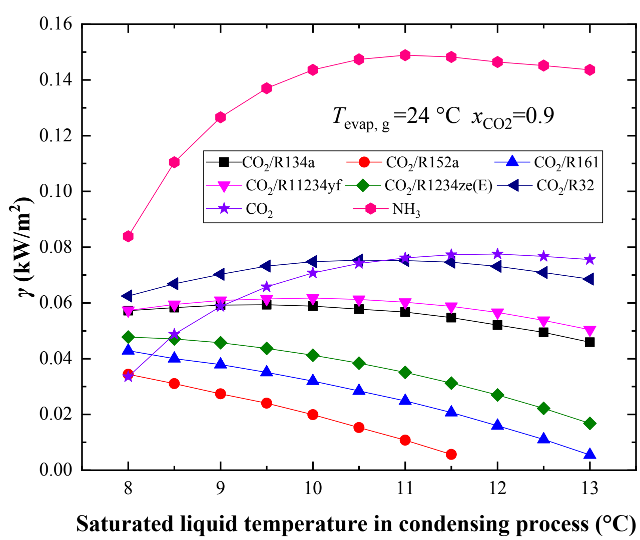

Fig. 15. Effects of condensing temperature on γ.

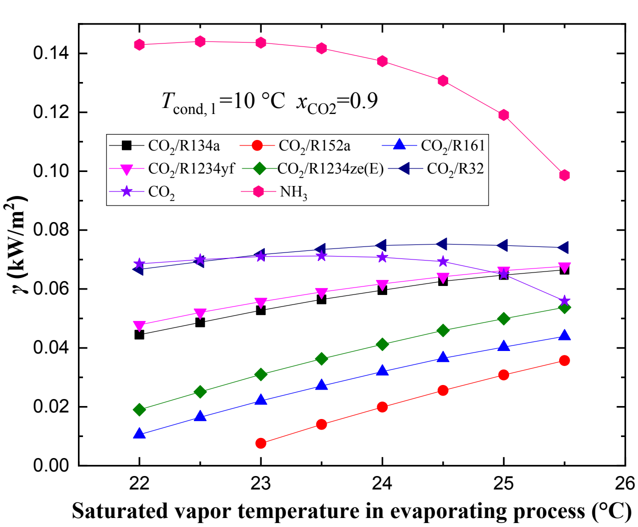

Fig. 14. Effects of evaporating temperature on γ.

taken for an example for mixtures. The figure shows that the value of γ first increases smoothly and decreases quickly with increasing evaporating temperature for pure CO_2 and NH_3. The value of γ for CO_2/R32 first increases and then decreases slightly after achieving an optimal value of 75.24 W/m^2 at T_{evap} of 24.5 °C. The curves of other mixtures show a tendency to increase with evaporating temperature. The is mainly due to fact that impact of total net power output causes more profound effect for mixtures, although both the heat transfer area and net power output increase with evaporating temperature·NH_3 clearly produces larger value of γ than other fluids, and the optimal value of 144.08 W/m^2 is obtained at T_{evap} of 22.5 °C. The temperature glide of mixtures could improve the thermodynamic, however, the improved thermal matching causes larger heat transfer areas. Besides, the mixtures have poorer heat transfer coefficient than NH_3, hence larger heat transfer areas are calculated for mixtures.

Among the mixtures, CO_2/R32 performs the best. To compare Fig. 14 with Fig. 15, the effect of condensing temperature shows a reversal trend·NH_3 also produces the maximum value of γ, and the optimal value is obtained at T_{cond} of 11 °C. These figures reveal that NH_3 is more profitable in respect to its higher value of γ. This founding is in consistent with previous works [3,12].

4. Other considerations

Different from conventional power cycles, the OTEC system produces fairly low thermal efficiency, and its thermodynamic performance exhibits more temperature sensitivity. The frictional pressure drop of working fluid may induces additional temperature change alone the heat exchange process, while the quantitative analysis of this influence is usually neglected in previous researches, including this work. In the point view of qualitative analysis, the pressure drop will certainly lead to the drop of saturated (evaporating/condensing) temperature, and the temperature drop is closely related to the saturated pressure. Working fluid with lower saturated pressure shows more dependence between pressure and temperature, for example, the saturated temperature change is about 3.28 °C (from 26 to 22.72 °C) for NH_3 with its pressure changing from 1.0345 MPa to 0.9345 MPa (pressure drop of 0.1 MPa). While for CO_2, the saturated temperature change is only 0.67 °C (from 26 to 25.33 °C) with its pressure changing from 6.584 MPa to 6.484 MPa (pressure drop of 0.1 MPa). Temperature drop in evaporating/condensing process caused by frictional pressure drop will lead to performance decline or even infeasibility for power cycle. Therefore, working fluids with higher saturated pressure, such as CO_2 and CO_2-based binary mixtures, show the property that its saturated temperature is more insensitive to pressure drop, and of more thermodynamic performance stability. Besides, as the *p-h* diagrams illustrate in Appendix C, CO_2-based binary mixtures exhibit much more lager pressure drop (more than 1 MPa) between turbine inlet and outlet which serves as driving force for power generation, while the pressure drop for NH_3 is only 0.5 MPa or even lower. An efficient compact turbine may benefit from the higher pressure and larger pressure drop.

In view of the low thermal efficiency, OTEC system requires large flow rates of seawater for power generation, therefore, the seawater pump power consumption has non-negligible influence. For the conventional Rankine cycle using pure working fluid, the temperature change of warm seawater is about 2–4 °C, while this value could achieve as much as 10 °C using CO_2-based binary mixtures, which means that cycle heat input could increase in several times under the same flow rate of seawater. Zeotropic mixtures with adequate temperature glide achieve good thermal matching with heat source/sink, and perform satisfactory thermodynamic performance. However, the lower mean temperature difference during heat exchange would result in increase of heat exchange area and corresponding component cost. The preliminary economic analysis ascertains mixtures produces lower γ value than NH_3. Nonetheless, optimization of main component size as well as detailed thermo-economic-environmental analysis for OTEC using CO_2-based mixtures remain to be further investigated in future.

5. Conclusions

In order to improve thermodynamic coupling of the OTEC power cycle and external warm/cold seawater, CO_2-based binary zeotropic mixtures are selected as promising working fluids. Rankine cycle using six CO_2-based mixtures as well as pure CO_2 and pure NH_3 are comprehensively optimized and comparatively investigated. The main conclusions can be summarized as follows:

(1) Rankine cycle using CO_2-based binary zeotropic mixtures could improve the thermal matching during heat exchange, temperature profiles of working fluid and external seawater could get nearly parallel. A deeper utilization of warm/cold seawater can be achieved, and temperature change of more than 10 °C and 7 °C could be realized for warm and cold seawater, respectively, rather higher than the value of about 4 °C for conventional cycle using pure working fluid. This verifies that Rankine cycle with CO_2-based binary zeotropic mixture serves close to a Lorenz cycle.
(2) The binary mixtures produce larger specific power output than pure working fluids. Among them, CO_2/R32 (0.76/0.24 wt%) produces the maximum value of 0.696 kJ/kg, nearly 38% higher than that of pure NH_3. The maximum system efficiency is achieved to be 3.32% by pure NH_3, higher than pure CO_2 and CO_2-based mixtures. Nonetheless, NH_3 outputs tiny specific power output at cycle design of maximum system efficiency.
(3) The performance of Rankine cycle is affected by the mixture composition. The maximum specific power output is achieved after synthetically considering cycle efficiency, thermal matching, and heat recovery ratio of external fluids by adjusting the temperature glide. The optimal composition of binary mixture is obtained when the evaporating temperature glide is about 7–8 °C in this case study.
(4) From the preliminary economic analysis, it can be concluded that NH_3 larger value of γ than other fluids, and the optimal value of 144.08 W/m^2 is obtained. Among the mixtures, CO_2/R32 performs the best.

Declaration of Competing Interest

The authors declare that they have no known competing financial interests or personal relationships that could have appeared to influence the work reported in this paper.

Acknowledgement

This work was supported by China Postdoctoral Science Foundation (No. 2018M641349) and Zibo City – Shandong University of Technology Cooperative Projects (No. 2019ZBXC081).

Appendix A. Mathematical model of heat exchangers

A plate heat exchanger with countercurrent arrangement is chosen for the OTEC system. The evaporator and condenser are assumed to have the same plate parameters, plate thickness of 0.6 mm, chevron angle of 60°. The length and the number of channels are selected to be the two degrees of freedom. The model for heat exchanger sizing process is based on reference [37].

The heat transfer rate for each section is calculated by:

$$\dot{Q} = U{\bullet}A{\bullet}LMTD \tag{A.1}$$

where LMTD is the logarithmic mean temperature difference.

The overall heat transfer coefficient is given by:

$$\frac{1}{U} = \frac{1}{\alpha_{\rm wf}} + \frac{\delta}{\lambda} + \frac{1}{\alpha_{\rm sw}} \tag{A.2}$$

where δ is the thickness and λ is the thermal conductivity of raw materials of the heat exchange plate, $\alpha_{\rm wf}$ and $\alpha_{\rm sw}$ are coefficient of heat transfer for the working fluid and seawater, respectively.

The convection heat transfer coefficient on each side of heat exchanger can be expressed as:

$$\alpha = \frac{\lambda{\bullet}Nu}{D_{\rm E}} \tag{A.3}$$

The frictional pressure drop of plate heat exchanger can be given by Eq. (19).

A.1. Single-phase flow

The heat transfer coefficient for single-phase can be determined by [38]:

$$\alpha = 0.428Re^{0.664}\,Pr^{1/3}\frac{\lambda}{D_{\rm E}} \tag{A.4}$$

where Re and Pr are the Reynolds Number and Prandtl Number (applicable for $1300 < Re < 3200$ and $4.74 < Pr < 5.12$), λ is the thermal conductivity of working fluid.

A.2. Two-phase flow

The evaporation heat transfer coefficient of working fluid can be calculated by [39]:

$$\alpha_{\rm eva} = 5.323Re_{\rm eq}^{0.42}Pr_{\rm l}^{1/3}\frac{\lambda_{\rm l}}{D_{\rm E}} \tag{A.5}$$

where $Re_{\rm eq}$ is the equivalent Reynolds numbers, which is given by:

$$Re_{\rm eq} = \frac{G_{\rm eq}D_{\rm E}}{\mu_l} \tag{A.6}$$

where $\mu_{\rm l}$ is dynamic viscosity [Pa·s], $G_{\rm eg}$ is the equivalent mass velocity, calculated by:

$$G_{\rm eq} = G\left(1-x + x\left(\frac{\rho_{\rm l}}{\rho_{\rm g}}\right)^{0.5}\right) \tag{A.7}$$

The Fanning friction factor of the condensation process is calculated by [40]:

$$f_{\rm eva} = 61000Re_{\rm eq}^{-1.25} \tag{A.8}$$

The condensation heat transfer coefficient of working fluid can be calculated by [41]:

$$\alpha_{\rm cond}{=}4.118Re_{\rm eq}^{0.4}{\rm Pr}_{\rm l}^{1/3}\frac{\lambda_{\rm l}}{D_{\rm E}} \tag{A.9}$$

The Fanning friction factor of the condensation process is calculated by Kuo correction:

$$f_{\rm cond} = 21500Re_{\rm eq}^{-1.14}Bo_{\rm eq}^{-0.085} \tag{A.10}$$

where $Bo_{\rm eq}$ are the equivalent Boiling numbers, which are given by:

$$Bo_{\rm eq} = \frac{q}{G_{\rm eq}r_{\rm fg}} \tag{A.11}$$

where q is average imposed wall heat flux [W/m^2], $r_{\rm fg}$ is enthalpy of vaporization [J/kg].

Appendix B. Flow chart of the simulation process

See Fig. A1.

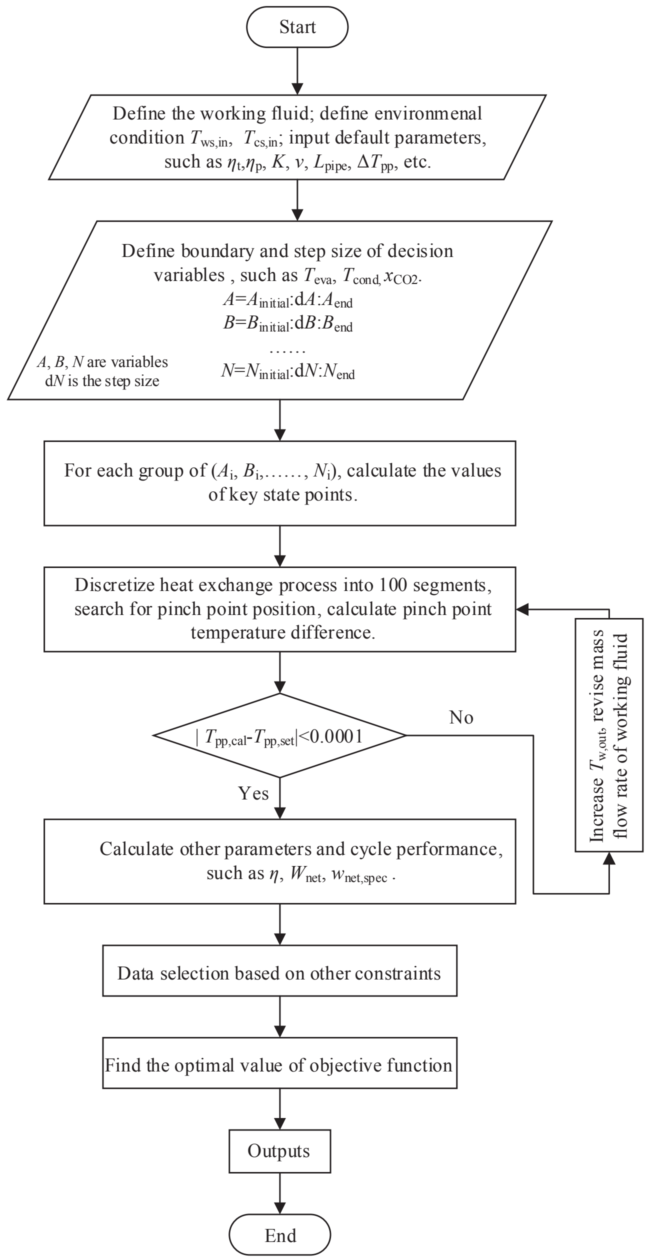

Fig. A1. Flow chart for thermodynamic simulation.

Appendix C. *p-h* diagrams for different working fluids

See Fig. A2.

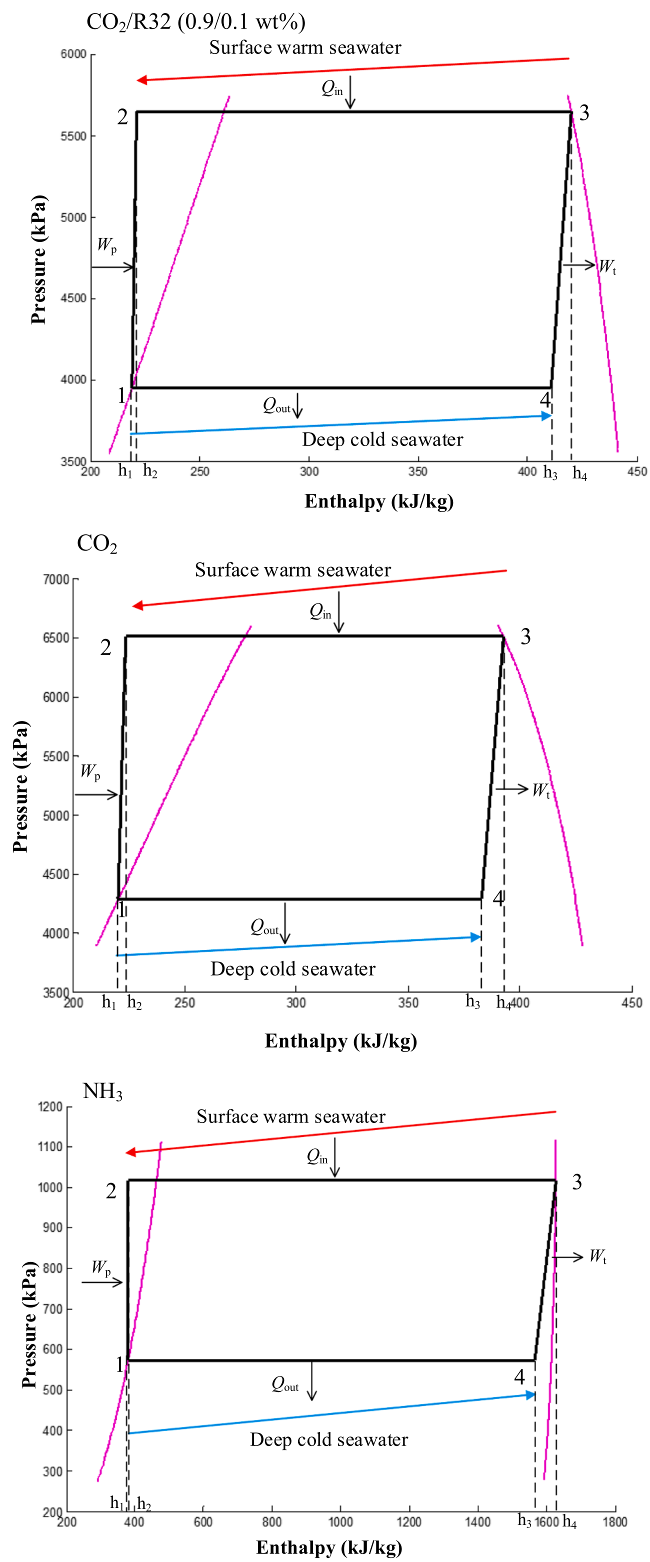

Fig. A2. *P-h* diagram of OTEC cycle. (a) CO_2/R32, (b) CO_2, (c) NH_3.

References

[1] K. Rajagopalan, Gérard C. Nihous, Estimates of global Ocean Thermal Energy Conversion (OTEC) resources using an ocean general circulation model, Renew. Energy 50 (2013) 532–540.
[2] F. McHale, W. Jones, H. Horn, Deployment and operation of the 50 kW mini-OTEC plant, OTC 3686, Offshore technology conference, Houston, (1980).
[3] C. Bernardoni, M. Binotti, A. Giostri, Techno-economic analysis of closed OTEC cycles for power generation, Renew. Energy 132 (2019) 1018–1033.
[4] V. Gudjónsdóttir, Analysis of external influences on an OTEC cycle, Mech. Eng. (2015).
[5] E. Brochard, The DCNS OTEC Roadmap for France, OTEC Roadmap for France; updated September 2015 OTEC by DCNS_September 2015 Update, OTEC Symposium–2015.
[6] H. Aydin, H.S. Lee, H.J. Kim, S. Shin, K. Park, Off-design performance analysis of a closed-cycle ocean thermal energy conversion system with solar thermal preheating and superheating, Renew. Energy 72 (2014) 154–163.
[7] H. Uehara, Y. Ikegami, Optimization of a closed-cycle OTEC system, J. Sol. Energy Eng. 112 (4) (1990) 247–256.
[8] H. Uehara, Y. Ikegami, T. Nishida, Performance analysis of OTEC system using a cycle with absorption and extraction processes, JSME 64 (624) (1998) 384–389.
[9] J. Yoon, S. Seol, C. Son, S. Jung, Y. Kim, H. Lee, H. Kim, J. Moon, Analysis of the high-efficiency EP-OTEC cycle using R152a, Renew. Energy 105 (2017) 366–373.
[10] I. Yasuyuki, Y. Takeshi, M. Takafumi, Ocean thermal energy conversion using double-stage rankine cycle, Mar. Sci. Eng. 6 (21) (2018) 1–18.
[11] F. Sun, Y. Ikegami, B. Jia, H. Arima, Optimization design and exergy analysis of organic Rankine cycle in ocean thermal energy conversion, Appl. Ocean Res. 35 (2012) 38–46.
[12] M. Yang, R. Yeh, Analysis of optimization in an OTEC plant using organic Rankine cycle, Renew. Energy 68 (3) (2014) 25–34.
[13] M. Wang, R. Jing, H. Zhang, C. Meng, N. Li, Y. Zhao, An innovative Organic Rankine Cycle (ORC) based Ocean Thermal Energy Conversion (OTEC) system with performance simulation and multi-objective optimization, Appl. Therm. Eng. 145 (2018) 743–754.
[14] J. Yoon, C. Son, S. Baek, H. Kim, H. Lee, Efficiency comparison of subcritical OTEC power cycle using various working fluids, Heat Mass Transf. 50 (7) (2014) 985–996.
[15] N. Kim, C. Kim, W. Chun, Using the condenser effluent from a nuclear power plant for Ocean Thermal Energy Conversion (OTEC), Int. Commun. Heat Mass Transfer 36 (2009) 1008–1013.
[16] N. Mohd Idrus, M. Musa, W. Yahya, A. Ithnin, Geo-ocean thermal energy conversion (GeOTEC) power cycle/plant, Renewable Energy 111 (2017) 372–380.
[17] N. Yamada, A. Hoshi, Y. Ikegami, Performance simulation of solar-boosted ocean thermal energy conversion plant, Renew. Energy 34 (7) (2009) 1752–1758.
[18] M. Faizal, M.R. Ahmed, Experimental studies on a closed cycle demonstration OTEC plant working on small temperature difference, Renew. Energy 51 (2013) 234–240.
[19] H. Yuan, N. Mei, S. Hu, et al., Experimental investigation on an ammonia-water based ocean thermal energy conversion system, Appl. Therm. Eng. 61 (2) (2013) 327–333.
[20] C. Vetter, H. Wiemer, D. Kuhn, Comparison of sub- and supercritical Organic Rankine Cycles for power generation from low-temperature/low-enthalpy geothermal wells, considering specific net power output and efficiency, Appl. Therm. Eng. 51 (1–2) (2013) 871–879.
[21] H. Yin, A. Sabau, J. Conklin, J. McFarlane, A. Qualls, Mixtures of SF_6-CO_2 as working fluids for geothermal power plants, Appl. Energy 106 (2013) 243–253.
[22] C. Wu, S. Wang, X. Jiang, J. Li, Thermodynamic analysis and performance optimization of transcritical power cycles using CO_2-based binary zeotropic mixtures as working fluids for geothermal power plants, Appl. Therm. Eng. 115 (2017) 292–304.
[23] E. Menon, Transmission Pipeline Calculations and Simulations Manual, 2015, pp. 1–599.
[24] K. Nilpueng, T. Keawkamrop, H. Ahn, S. Wongwises, Effect of chevron angle and surface roughness on thermal performance of single-phase water flow inside a plate heat exchanger, Int. Commun. Heat Mass Transfer 91 (2018) 201–209.
[25] L. Pan, W. Shi, Investigation on the pinch point position in heat exchangers, J. Therm. Sci. 3 (2016) 258–265.
[26] E. Cayer, N. Galanis, M. Desilets, H. Nesreddine, P. Roy, Analysis of a carbon dioxide transcritical power cycle using a low temperature source, Appl. Energy 86 (7–8) (2009) 1055–1063.
[27] L. Pan, Y. Ma, T. Li, H. Li, B. Li, X. Wei, Investigation on the cycle performance and the combustion characteristic of two CO_2-based binary mixtures for the transcritical power cycle, Energy 179 (2019) 454–463.
[28] P. Garg, P. Kumar, K. Srinivasan, P. Dutta, Evaluation of carbon dioxide blends with isopentane and propane as working fluids for organic Rankine cycles, Appl. Therm. Eng. 52 (2) (2013) 439–448.
[29] E.W. Lemmon, M.O. McLinden, M.L. Huber, Reference fluid thermodynamic and transport properties database (REFPROP), NIST Standard Reference Database 23, Version 9.0. Gaithersburg, MD: National Institute of Standards and Technology (NIST), 2010.
[30] ANSL/ASHRAE Standard 34-2010 - Designation and Safety Classification of Refrigerants. Atlanta: ASHRAE, 2010.
[31] L. Cai, Performance evaluation and parametric optimum design of an updated ocean thermal energy conversion system, Ocean Eng. 117 (2016) 254–258.
[32] F. Sinama, M. Martins, A. Journoud, O. Marc, F. Lucas, Thermodynamic analysis and optimization of a 10MW OTEC Rankine cycle in Reunion Island with the equivalent Gibbs system method and generic optimization program GenOpt, Appl. Ocean Res. 53 (2015) 54–66.
[33] J. Yoon, C. Son, S. Baek, B. Ye, H. Kim, H. Lee, Performance characteristics of a high-efficiency R717 OTEC power cycle, Appl. Therm. Eng. 72 (2014) 304–308.
[34] Hüseyin Yağlı, Yıldız Koç, Ali Koç, Adnan Görgülü, Ahmet Tandiroğlu, Parametric optimization and exergetic analysis comparison of subcritical and supercritical organic Rankine cycle (ORC) for biogas fuelled combined heat and power (CHP) engine exhaust gas waste heat, Energy 111 (2016) 923–932.
[35] R. Soto, J. Vergara, Thermal power plant efficiency enhancement with ocean thermal energy conversion, Appl. Therm. Eng. 62 (1) (2014) 105–112.
[36] R. Yeh, T.Z. Su, M.S. Yang, Maximum output of an OTEC power plant, Ocean Eng. 32 (5–6) (2005) 685–700.
[37] S. Quoilin, S. Declaye, B. Tchanche, V. Lemort, Thermo-economic optimization of waste heat recovery Organic Rankine Cycles, Appl. Therm. Eng. 31 (2011) 2885–2893.
[38] K. Nilpueng, S. Wongwises, Experimental study of single-phase heat transfer and pressure drop inside a plate heat exchanger with a rough surface, Exp. Therm Fluid Sci. 68 (2015) 268–275.
[39] I. Kim, J. Park, Y. Kwon, Y. Kim, Experimental study on R-410A evaporation heat transfer characteristics in oblong shell and plate heat exchanger, Heat Transfer Eng. 28 (7) (2007) 633–639.
[40] Y. Hsieh, T. Lin, Saturated flow boiling heat transfer and pressure drop of refrigerant R-410A in a vertical plate heat exchanger, Int. J. Heat Mass Transf. 45 (5) (2002) 1033–1044.
[41] Y. Yan, H. Lio, T. Lin, Condensation heat transfer and pressure drop of refrigerant R-134a in a plate heat exchanger, Int. J. Heat Mass Transf. 42 (1999) 993–1006.